The Role of Clouds in Shaping Tropical Pacific Response Pattern to Extratropical Thermal Forcing

Wei-Ting Hsiao[1], Yen-Ting Hwang[2], Yong-Jhih Chen[2], and Sarah M. Kang[3]

[1]Colorado State University
[2]National Taiwan University
[3]Ulsan National Institute of Science and Technology

November 25, 2022

Abstract

Extratropical influences on tropical sea surface temperature (SST) have implications for decadal predictability. We implement a cloud-locking technique to highlight the critical role of clouds in shaping tropical SST response to extratropical thermal forcing. With heating imposed over either extratropical Northern Atlantic or Pacific, Hadley Cells respond similarly that the trades strengthen south of the rainband. The wind-evaporation-SST (WES) feedback leads to cooling over the southern subtropics, which is enhanced in the southeastern Pacific due to the positive feedback between SST and stratiform clouds. This cooling is further extended toward the central Pacific via a WES effect associated with zonally contrasting cloud-radiative-SST feedbacks in the tropics, which is observed in both slab-ocean and dynamical-ocean experiments. We propose that the meridional and zonal SST gradients are tightly linked via WES effects and the cloud-radiative-SST feedbacks, which are largely determined by the climatological rainband position and the spatial distribution of cloud properties.

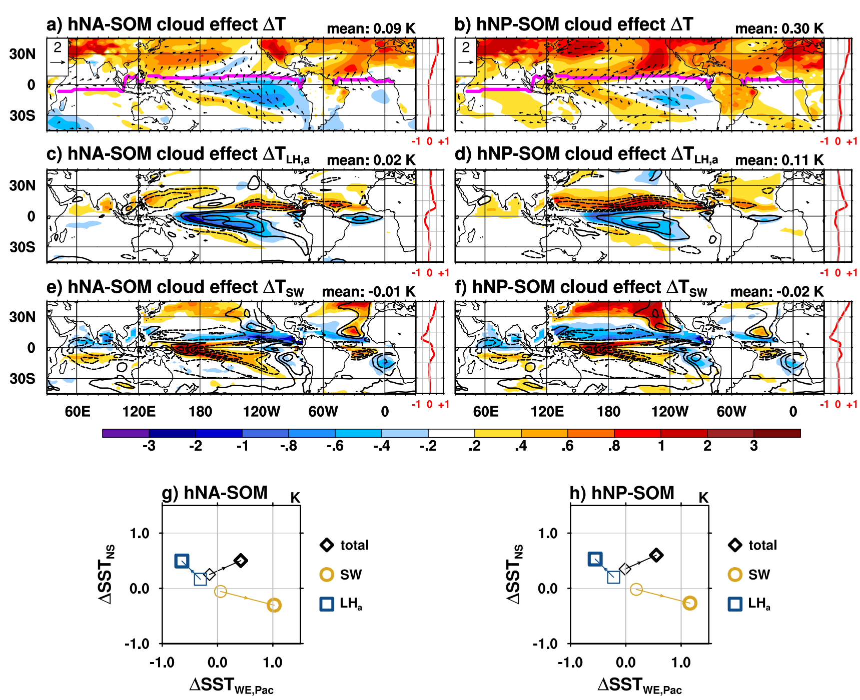

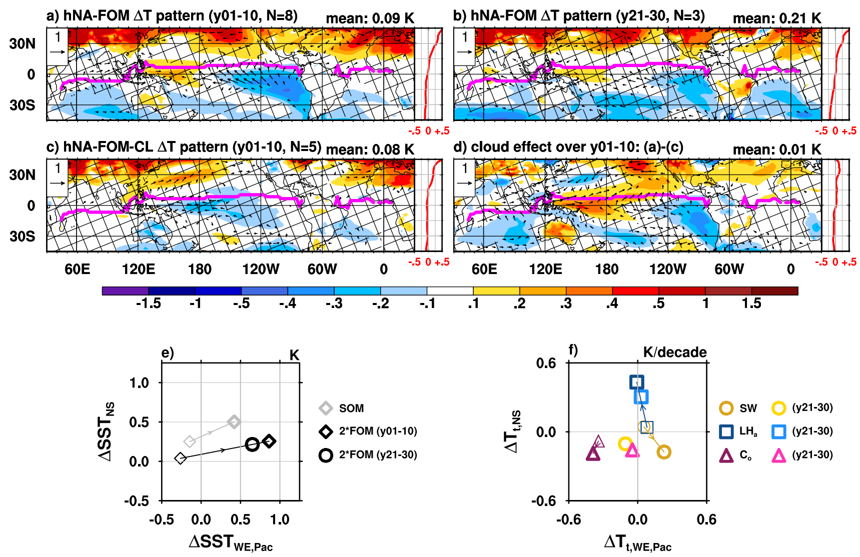
a) hNA-FOM ΔT pattern (y01-10, N=8)
mean: 0.09 K
b) hNA-FOM ΔT pattern (y21-30, N=3)
mean: 0.21 K
c) hNA-FOM-CL ΔT pattern (y01-10, N=5)
mean: 0.08 K
d) cloud effect over y01-10: (a)-(c)
mean: 0.01 K
30N
0
30S
60E
120E
180
120W
60W
0
-.5 0 +.5
-1.5 -1 -.5 -.4 -.3 -.2 -.1 .1 .2 .3 .4 .5 1 1.5
e)
K
ΔSST_NS
ΔSST_WE,Pac
SOM
2*FOM (y01-10)
2*FOM (y21-30)
f)
K/decade
ΔT_t,NS
ΔT_t,WE,Pac
SW
LH_a
C_o
(y21-30)

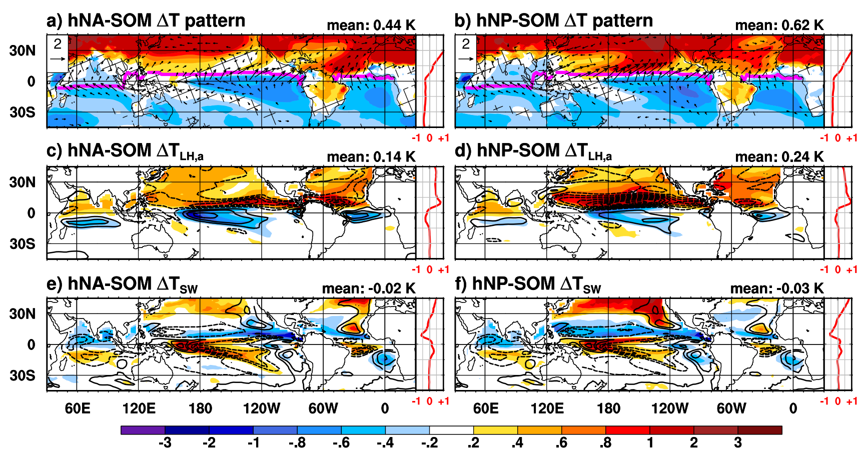
a) hNA-SOM ΔT pattern
mean: 0.44 K
b) hNP-SOM ΔT pattern
mean: 0.62 K
c) hNA-SOM ΔT_LH,a
mean: 0.14 K
d) hNP-SOM ΔT_LH,a
mean: 0.24 K
e) hNA-SOM ΔT_SW
mean: -0.02 K
f) hNP-SOM ΔT_SW
mean: -0.03 K
30N
0
30S
60E
120E
180
120W
60W
0
-1 0 +1
-3 -2 -1 -.8 -.6 -.4 -.2 .2 .4 .6 .8 1 2 3

Figure 1.

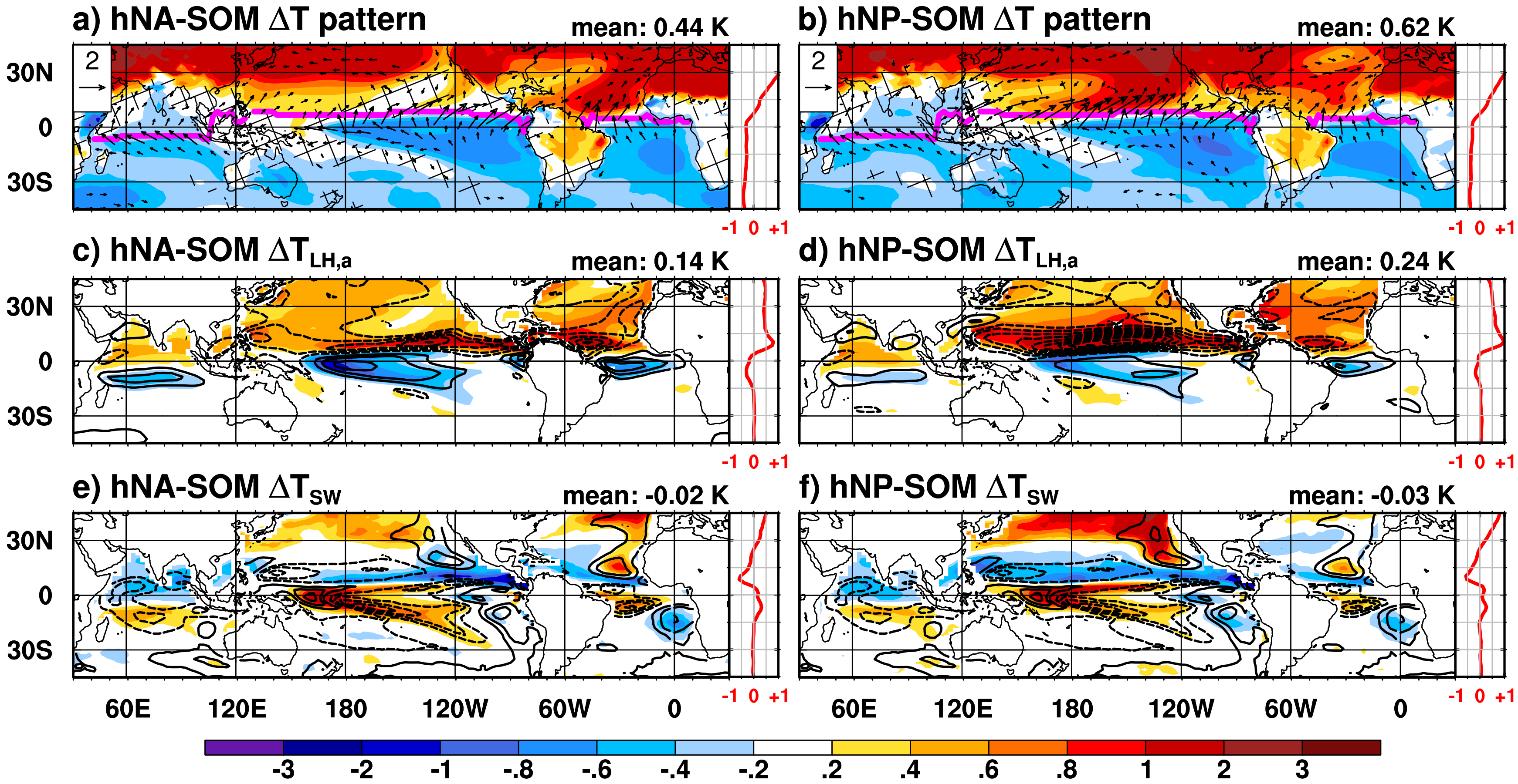

a) hNA-SOM ΔT pattern
mean: 0.44 K
b) hNP-SOM ΔT pattern
mean: 0.62 K
c) hNA-SOM ΔT$_{LH,a}$
mean: 0.14 K
d) hNP-SOM ΔT$_{LH,a}$
mean: 0.24 K
e) hNA-SOM ΔT$_{SW}$
mean: -0.02 K
f) hNP-SOM ΔT$_{SW}$
mean: -0.03 K
2
30N
0
30S
60E 120E 180 120W 60W 0
-1 0 +1
-3 -2 -1 -.8 -.6 -.4 -.2 .2 .4 .6 .8 1 2 3

Figure 2.

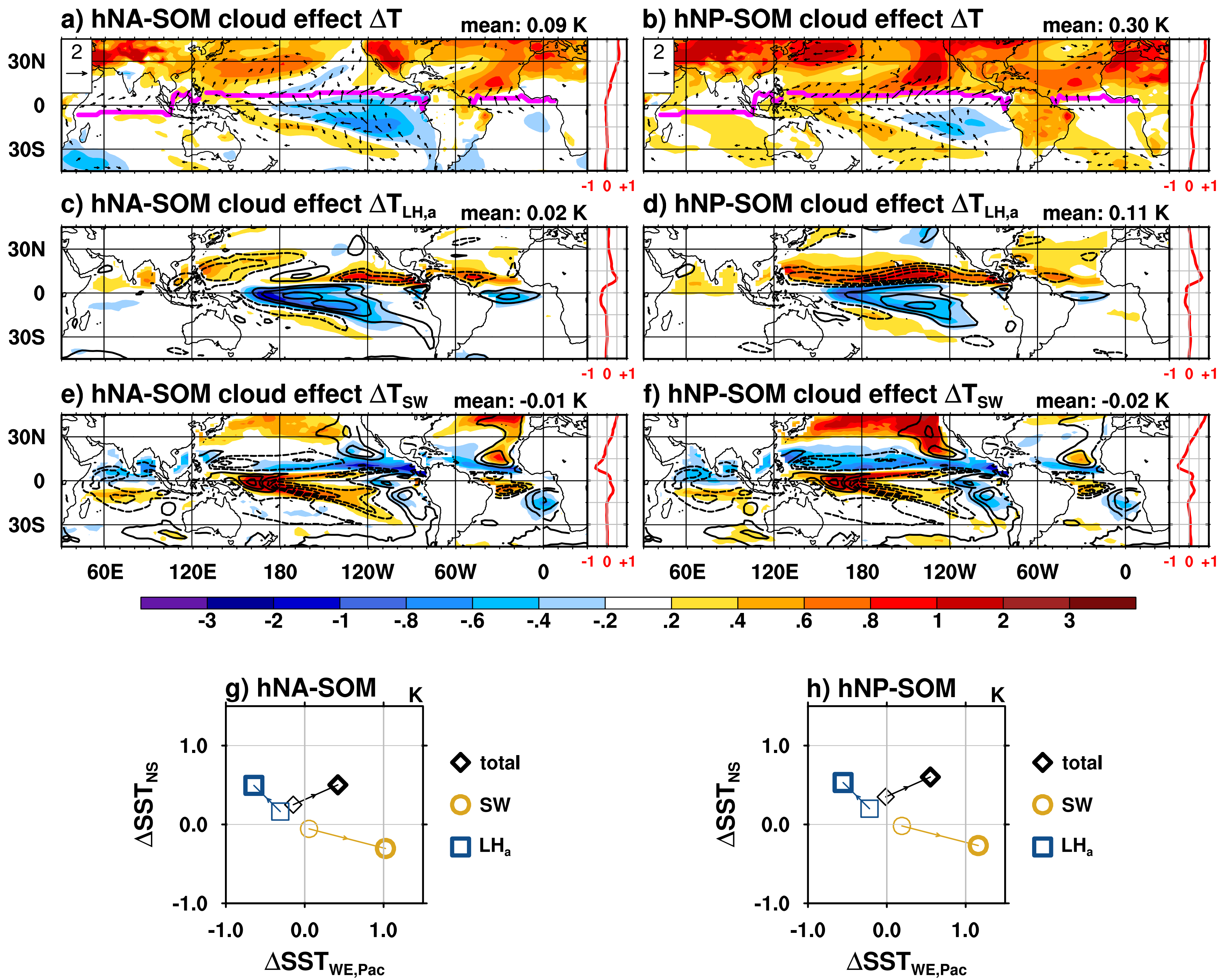

a) hNA-SOM cloud effect ΔT
mean: 0.09 K
b) hNP-SOM cloud effect ΔT
mean: 0.30 K
c) hNA-SOM cloud effect $\Delta T_{LH,a}$
mean: 0.02 K
d) hNP-SOM cloud effect $\Delta T_{LH,a}$
mean: 0.11 K
e) hNA-SOM cloud effect ΔT_{SW}
mean: -0.01 K
f) hNP-SOM cloud effect ΔT_{SW}
mean: -0.02 K
30N
0
30S
60E
120E
180
120W
60W
0
-1 0 +1
2
-3 -2 -1 -.8 -.6 -.4 -.2 .2 .4 .6 .8 1 2 3
g) hNA-SOM
h) hNP-SOM
K
1.0
0.0
-1.0
ΔSST_{NS}
$\Delta SST_{WE,Pac}$
total
SW
LH_a

Figure 3.

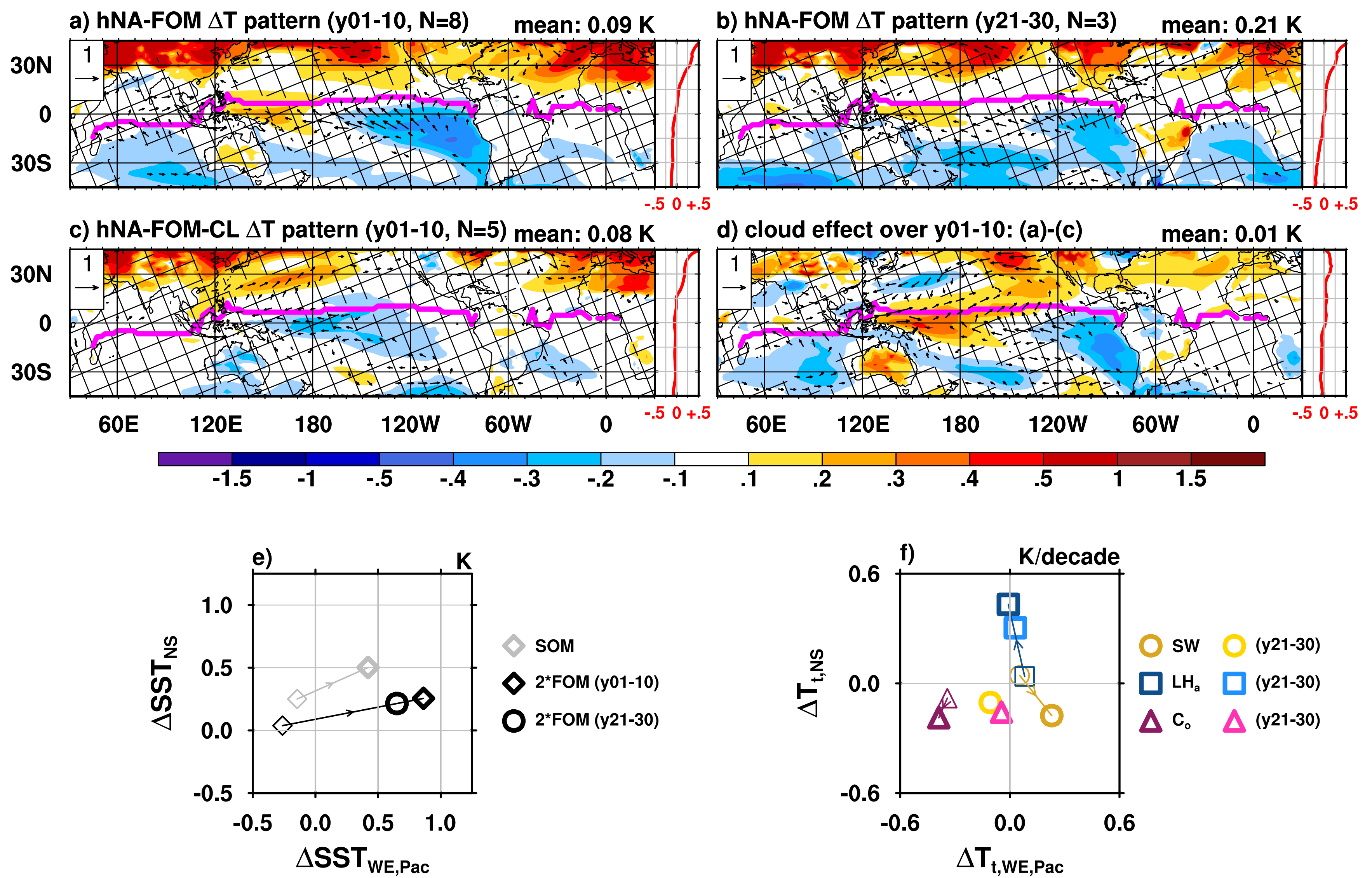
a) hNA-FOM ΔT pattern (y01-10, N=8)
mean: 0.09 K
b) hNA-FOM ΔT pattern (y21-30, N=3)
mean: 0.21 K
c) hNA-FOM-CL ΔT pattern (y01-10, N=5)
mean: 0.08 K
d) cloud effect over y01-10: (a)-(c)
mean: 0.01 K
30N
0
30S
60E
120E
180
120W
60W
-.5 0 +.5
-1.5 -1 -.5 -.4 -.3 -.2 -.1 .1 .2 .3 .4 .5 1 1.5
e)
K
ΔSST_{NS}
$\Delta SST_{WE,Pac}$
SOM
2*FOM (y01-10)
2*FOM (y21-30)
f)
K/decade
$\Delta T_{t,NS}$
$\Delta T_{t,WE,Pac}$
SW
(y21-30)
LH_a
(y21-30)
C_o
(y21-30)

Figure 4.

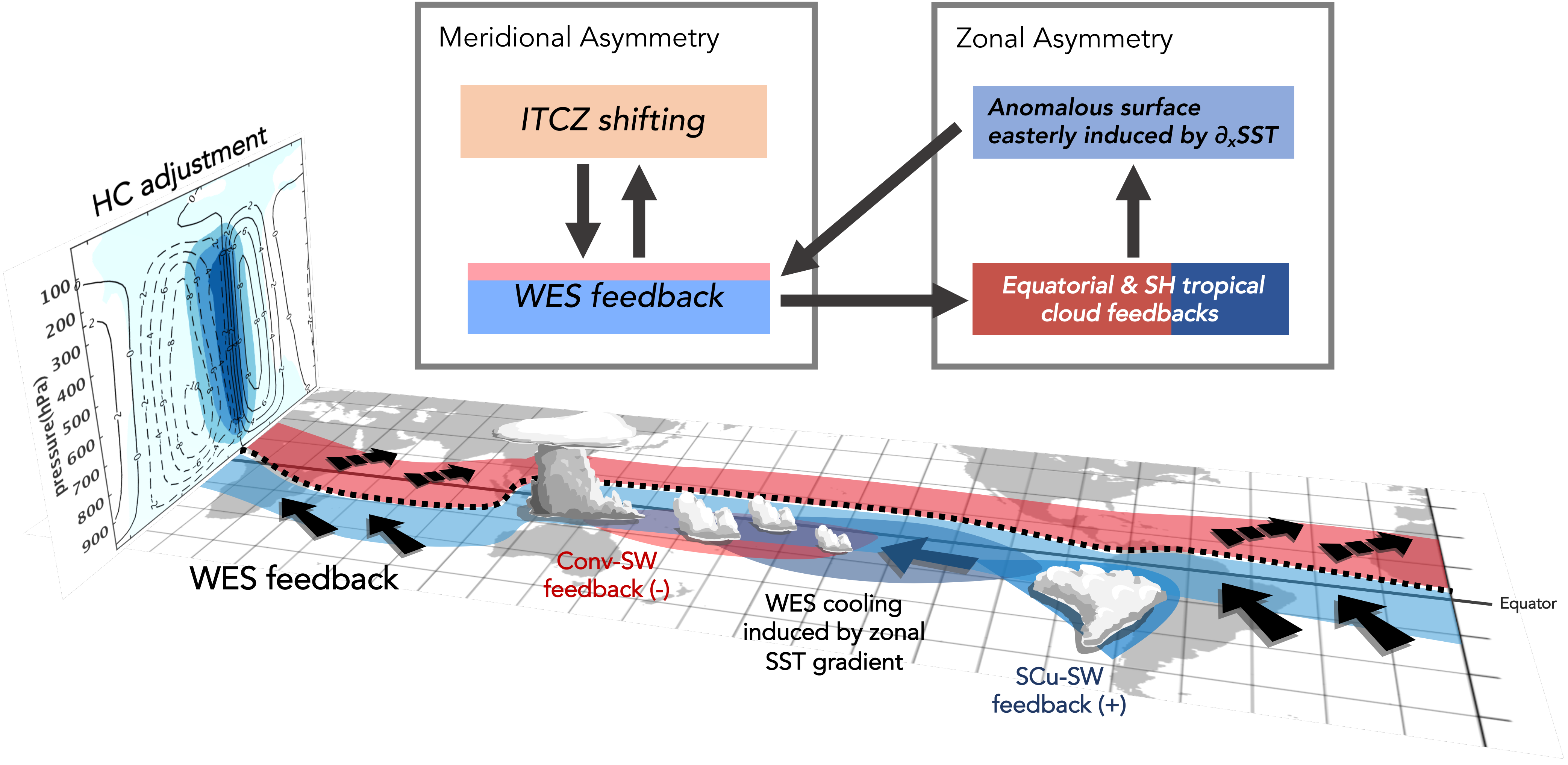

Meridional Asymmetry
ITCZ shifting
WES feedback
Zonal Asymmetry
Anomalous surface easterly induced by $\partial_x SST$
Equatorial & SH tropical cloud feedbacks
HC adjustment
pressure(hPa)
100
200
300
400
500
600
700
800
900
WES feedback
Conv-SW feedback (-)
WES cooling induced by zonal SST gradient
SCu-SW feedback (+)
Equator

The Role of Clouds in Shaping Tropical Pacific Response Pattern to Extratropical Thermal Forcing

Wei-Ting Hsiao[1,2], Yen-Ting Hwang[1], Yong-Jhih Chen[1], and Sarah M. Kang[3]

[1]Department of Atmospheric Sciences, National Taiwan University, Taipei, Taiwan
[2]Department of Atmospheric Science, Colorado State University, Fort Collins, CO, USA
[3]School of Urban and Environmental Engineering, Ulsan National Institute of Science and Technology, Ulsan, South Korea

Key Points:

- Tropical surface temperature responds similarly to idealized heating imposed over either North Atlantic or North Pacific as fast response
- Clouds are essential in forming the tropical response pattern through their coupling with circulation and surface energy fluxes
- The climatological rainband position in the tropics determines how clouds shape the tropical responses to extratropical forcing

Corresponding author: Yen-Ting Hwang, `ythwang@ntu.edu.tw`

Abstract

Extratropical influences on tropical sea surface temperature (SST) have implications for decadal predictability. We implement a cloud-locking technique to highlight the critical role of clouds in shaping tropical SST response to extratropical thermal forcing. With heating imposed over either extratropical Northern Atlantic or Pacific, Hadley Cells respond similarly that the trades strengthen south of the rainband. The wind-evaporation-SST (WES) feedback leads to cooling over the southern subtropics, which is enhanced in the southeastern Pacific due to the positive feedback between SST and stratiform clouds. This cooling is further extended toward the central Pacific via a WES effect associated with zonally contrasting cloud-radiative-SST feedbacks in the tropics, which is observed in both slab-ocean and dynamical-ocean experiments. We propose that the meridional and zonal SST gradients are tightly linked via WES effects and the cloud-radiative-SST feedbacks, which are largely determined by the climatological rainband position and the spatial distribution of cloud properties.

Plain Language Summary

Tropical sea surface temperature could induce changes in global climate patterns, and could be impacted by climate perturbation at mid-to-high latitudes on decadal timescales. Understanding how the tropics and extratropics interact could help predict the decadal evolution of the climate. We examine such interaction with a global climate model. Common tropical climate response patterns to the heating imposed in either extratropical Northern Atlantic or Pacific are found, determined by the following mechanisms. First, the wind speed of the trades responds in opposite manners with respect to the mean-state tropical rainband, where stronger trades and surface evaporation is present over the equator and its south that cools the sea surface. Second, this equatorial cooling is stronger over the eastern Pacific, which is associated with the mean-state properties of how clouds interact with changing surface temperature, that convective clouds over the western and central Pacific tend to damp the change, while stratiform clouds over the eastern Pacific act to amplify the change. These mechanisms, which are largely established by the mean-state rainband position and the spatial distribution of cloud properties, act to link the zonal and meridional structure of the sea surface temperature over the tropical Pacific.

1 Motivation

Tropical Pacific sea surface temperature (SST) has far-reaching climate impacts with its direct influences on atmospheric convection and thus planetary-scale stationary Rossby waves. For example, the La Niña-like cooling trend during 1998-2012 is suggested to affect the global distribution of rainfall and the occurrences of tropical storms (Delworth et al., 2015; Zhao et al., 2018). Through its critical modulation of the vertical structures of tropical atmospheric temperature and thus the efficiency of radiative climate feedbacks, the temporal evolution of tropical Pacific SST pattern is reported to control the climate sensitivity in observational records and modeling simulations (e.g. Andrews et al., 2015; Ceppi & Gregory, 2017; Dong et al., 2019), often referred to as “the pattern effect” (Stevens et al., 2016).

With the increasing demands for decadal climate predictability upon anthropogenic influences, driving mechanisms behind tropical Pacific SST trends under warming scenarios have been proposed, but have yet been comprehensively understood (Collins et al., 2018; Xie, 2020). The role of ocean dynamics in modulating the SST pattern on diverse timescales is well recognized via a coupling between the oceanic temperature structures and oceanic currents driven by atmospheric wind stress (Clement et al., 1996; Heede et al., 2020). In this study, the air-sea heat flux is of interest since recent literature has shown their major roles in affecting the SST under anthropogenic climate change. For instance, the spatial structure of evaporation, which is largely determined by surface winds, shapes the anomalous SST pattern with increased CO_2 (L. Wang & Huang, 2016; Xie et al., 2010). Cloud radiative feedbacks, which are established by cloud properties associated with atmospheric circulations and the SST pattern itself, could also impose radiative flux anomalies and SST tendencies over the tropical Pacific (DiNezio et al., 2009).

Recently, the non-local extratropical effects in driving tropical Pacific SST trends have received increasing attention. Couplings between atmospheric adjustments, surface fluxes, and oceanic tunnels could translate anomalies in the extratropics into tropical Pacific SST changes (Amaya et al., 2019; Luo et al., 2017; Shin et al., 2021; Hwang et al., 2021). Localized energy perturbations are commonly present in the extratropics, such as those due to anthropogenic aerosol emissions and polar sea ice losses. Localized forcing in the extratropics have been found to be homogenized zonally before propagating through the atmosphere into the tropics by subtropical eddies, making tropical response insensitive to the exact locations of the forcing (Kang et al., 2014, 2018; L'Hévéder et al., 2015). In particular, Kang et al. (2018) proposed that in a slab-ocean climate model, a common La Niña-like response pattern appears along with the northward displacement of the ITCZ in response to Northern Hemispheric differential heating at different locations in the extratropics.

This study investigates the formation mechanisms behind such La Niña-like tropical SST pattern response to localized extratropical thermal forcing from Kang et al. (2018). Later in this paper, we show that the formation of such pattern is established by the climatological rainband position and the climatological spatial pattern of cloud radiative feedbacks (Section 3). This is supported by cloud-locking experiments and is relevant in both models with a slab ocean and a fully coupled dynamical ocean (Section 4). We suggest that these climatological controls on tropical Pacific SST response to extratropical forcing could be applied to other forcing scenarios and offer potential source of predictive skills of the SST on decadal timescales (Section 5).

2 Methodology

2.1 Experimental Design

Sets of a control and two perturbed experiments are performed with Community Atmosphere Model 5.0 (CAM5; Neale et al., 2010) with Community Earth System Model 1.2 (Hurrell et al., 2013). Anomalous surface flux convergence is imposed into the equilibrated preindustrial simulations (CTL) between 45°N and 65°N zonally uniformly in either the North Atlantic (hNA) or North Pacific (hNP), each with a total amount of 0.41 petawatts. The climate responses to heating are defined as the time-averaged fields from either heating deducted by those from CTL. See Table S1 and Text S1 for a full list of experiments and a detailed explanation of the experimental design.

To investigate the SST formation mechanisms driven solely by surface fluxes, a slab-ocean model (SOM) with a constant mixed-layer depth of 50 meters is coupled to CAM5. Thirty years of data are analyzed after a spinning up of thirty-five years. To evaluate whether the proposed feedbacks shown in the SOM experiments remain important when oceanic processes are involved, experiments using a full-depth dynamical ocean model (FOM) are performed. The averaged hNA response of eight ensembles over years 1-10 and three ensembles over years 21-30 are analyzed. Fewer ensembles of the hNP experiments in FOM are also conducted but are only shown in Figure S1 for brevity, while their results are consistent with the main conclusions.

The other two sets of experiments are conducted to assess the direct and indirect impact of cloud radiative effects. A cloud-locking (CL) technique is used (Ceppi & Hartmann, 2016; Y.-J. Chen et al., 2021), in which hourly cloud optical properties from CTL are prescribed in CAM5. The SOM cloud-locking simulations are performed with preindustrial condition (CTL) and with either of the heating. The control run is spun up for ten years while the perturbed runs are spun up for twenty years, and the following twenty years are analyzed in all runs. The FOM cloud-locking simulations are performed with only the North Atlantic heating and with five ensembles running out to ten years. We define the *cloud effect* by subtracting the responses in experiments with locked clouds from those with interactive clouds.

2.2 Energetic decomposition of SST response

An energy budget analysis of oceanic mixed layer is used to attribute SST response to surface energy fluxes (Xie et al., 2010; L. Zhang & Li, 2014). Briefly, the time tendency of the mixed-layer temperature (T) can be written as:

$$T_t = \frac{1}{\rho c_p H}\left(Q_{SW} + Q_{LW} + Q_{LH} + Q_{SH} + Q_{C_o}\right) \tag{1}$$

where the subscript t denotes a time derivative, ρ the density of sea water, c_p the specific heat capacity of sea water at constant pressure, H the mixed-layer depth, and Q the inward energy flux. Fluxes include shortwave (SW) and longwave (LW) radiative fluxes, latent heat flux (LH), sensible heat flux (SH), and column-integrated heat convergence by oceanic heat transport (C_o). T_t contributed by each energy flux term can be written as:

$$T_{t,flux} = \frac{1}{\rho c_p H} Q_{flux}, \;\; flux = \{SW, LW, LH, SH, C_o\} \tag{2}$$

In FOM experiments, $T_{t,flux}$ are calculated to show the contribution of fluxes to the trend of T with an averaged H used. In SOM experiments, Q_{C_o} is unchanged by design and the system reaches equilibrium thus $T_t = 0$. The temperature difference between the control state and the forced states in SOM runs can then be written as:

$$\Delta T_{flux} = \frac{1}{\overline{dQ/dT}} \Delta Q_{flux}, \;\; flux = \{SW, LW_{dn}, LH_a, SH\} \tag{3}$$

where Δ denotes the differences between the forced and the control states, and $\overline{dQ/dT}$ is the linear dependence of total surface energy flux to T evaluated at the arithmetic-mean states between the forced and the control states, which consists of a blackbody longwave radiative term and a latent heat term associated with its bulk formula. After removing the linear dependent terms to T, downward longwave radiative flux (LW_{dn}) and non-Newtonian latent heat flux that depends solely on near-surface atmospheric condition (LH_a) appear that replace LW and LH, respectively. Finally, ΔT_{flux} are calculated to show the contribution of the change in fluxes to the change in T. See Text S2 for a detailed derivation and expression of each term.

3 The climatological controls of the response patterns

We first present the responses in SOM experiments. Regardless of heating being imposed in either North Atlantic or North Pacific, steady-state surface temperature response patterns are highly similar, with a spatial correlation of 0.86 within 30°S and 30°N (comparing Figure 1a with 1b). Both the interhemispheric and zonal SST gradients strengthen along the equatorial Pacific. Responding to the imposed heating in the Northern Hemisphere, an anomalous cross-equatorial overturning circulation develops to transport energy southward through its upper branch and to shift moisture and the ITCZ northward through its lower branch (shown by the low-level wind response in Figures 1a-b). The robust similarities of the tropical responses are consistent with Kang et al. (2018) who proposed that extratropical forcing is being homogenized before affecting the tropics.

First, we discuss the formation mechanism behind the anomalous meridional SST structure, which is largely established by the climatological position of the tropical rainband (pink lines in Figures 1a-b). The climatological rainband is located at the transition region between the northeast and the southeast trades. With the rainband shifts

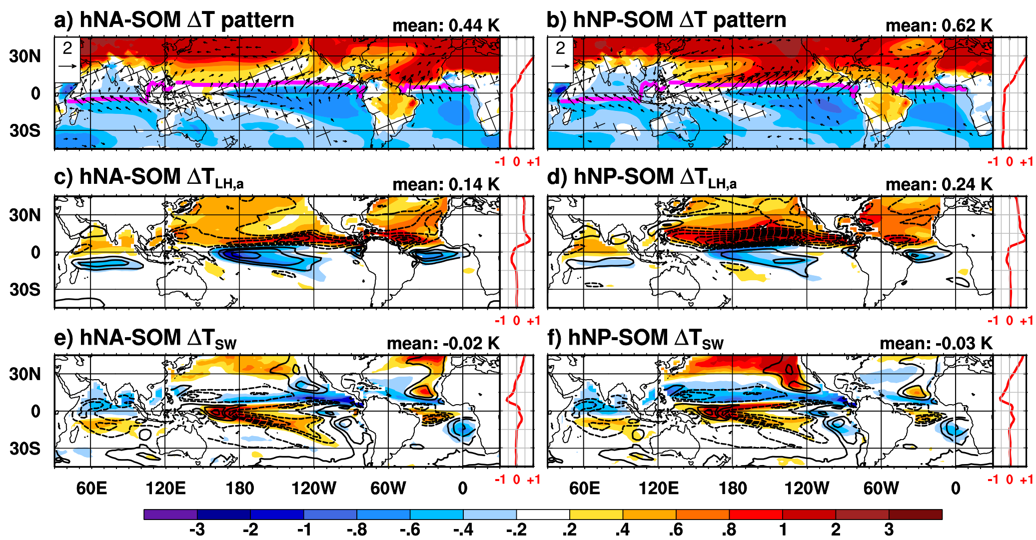

Figure 1. (a-b) responses of surface temperature pattern (shading; K) and 993-hPa winds (arrows), with climatological ITCZ defined at where the annual rainfall on marine region has meridional maxima (pink line), and the hatched regions show where the shading patterns are statistically insignificant at 5% level using two-tailed Student t-tests. In (c-d), shading shows $\Delta T_{LH,a}$ (units: K) and contours show the response of 10-meter wind speeds (spacing: 0.2 m s^{-1}). In (e-f), shading shows ΔT_{SW} (units: K) and contours show the surface SW-SST feedbacks estimated as the slope from the linear regression of surface shortwave radiative flux on SST using CTL-SOM (spacing: 5 W m^{-2} K^{-1}). The patterns of responses are calculated by removing their means over 30°S-30°N. Mean values of the shadings over 30°S-30°N are labeled, and zonal mean values of the shadings are attached on the right of each panel. For contours, dashed indicates negative, solid indicates positive, and zero lines are omitted.

toward the north in response to the Northern Hemispheric heating, anomalous low-level southerlies dominate over the tropics, which strengthen the southeasterlies on the south of the rainband and result in increased evaporation (negative $\Delta T_{LH,a}$) and cooler SST, while the opposite is shown in the north. This dipole pattern of $\Delta T_{LH,a}$ dominates the response of the anomalous meridional SST structure, while it is partly damped by the shortwave radiative effect (ΔT_{SW}; Figures 1e-f) associated with the shift of the rainband. As the rainband shifts toward the warmer Northern Hemisphere, the response of cloud cover and shortwave reflectivity are anti-symmetric to the climatological rainband, leading to cooling on the north and heating on the south.

The role of climatological rainband in determining the center of the meridional dipole SST response is consistent with previous literature (e.g. Chiang & Bitz, 2005), known as the ITCZ blocking effect, stating that anomalous warming is not able to penetrate the climatological rainband and could even induce an anomalous cooling south of the rainband. Kang et al. (2020) further demonstrate that the climatological ITCZ location acts as a barrier to the propagation of the surface temperature anomalies in response to extratropical forcing using a set of aqua-planet experiments. This effect produced by the climatological rainband is also shown in natural variabilities, as H. Zhang et al. (2014) suggest that the anomalous SST and surface winds associated with the South Pacific Meridional Mode no longer reach the equatorial region under a climatological state with the rainband located south of the equator.

Next, we turn our attention to the mechanism behind the enhanced zonal SST gradient over the equatorial Pacific, which is established by the spatial structure of climatological cloud regimes. The response of cloud cover under different environments to the latent heat cooling across the equatorial region shapes the zonal structure of the SST response. Shown as the contours in Figures 1e-f, shortwave-SST feedback over the tropics is positive over the east of the basins where stratiform clouds prevail and is negative along the convective ITCZ and the South Pacific Convergence Zone. With increased low-level atmospheric stability followed by the decrease in SST, marine stratiform clouds increase over the eastern equatorial Pacific (Hanson, 1991; Klein & Hartmann, 1993). Associated with the anomalous cross-equatorial Hadley Cell, the strengthened subtropical high in South Pacific may also produce anomalous cold advection and further increase the marine stratiform clouds (Wei et al., 2018). In contrast, the decreased SST and strengthened subsidence both inhibit deep convections and anvil clouds over the western-central tropical Pacific, allowing more solar insolation to heat up the surface (Lau et al., 1997; Ramanathan & Collins, 1991; Meehl & Washington, 1996). Distinct cloud radiative-SST feedback in the eastern and western equatorial Pacific is recently highlighted in Park et al. (2022). These zonally contrasting cloud-radiative feedbacks appear to be the most dominant term that contributes positively to the enhanced zonal SST gradient over the equatorial Pacific (comparing ΔT_{SW} in Figures 1e-f with Figures 1a-b). The contributions from longwave and sensible heat fluxes are at less importance in shaping the overall SST response pattern (not shown), whereas $\Delta T_{LH,a}$ serves as the main damping term of the zonal SST gradient response.

4 The coupling between clouds and circulation

In Section 3, we suggest the mechanisms underlying the similar pattern of SST response over the tropical Pacific, considering their dependence on climatology. Namely, the northward displacement of the tropical rainband and the zonal contrast in the climatological cloud regimes together shape the tropical SST pattern response to the extratropical thermal forcing. In this section, we use a cloud-locking technique (see Section 2) to verify the role of clouds in shaping the structure of the SST response.

The enhanced zonal SST gradient over the equatorial Pacific is mostly contributed by the *cloud effect* (as defined in Section 2), which is obtained by comparing simulations with interactive and locked cloud radiative properties. As shown in the scatter plots in Figures 2g-h, the changes in the equatorial Pacific zonal SST gradient are close to zero or even negative in the cloud-locking simulations (thin black diamond), whereas they are largely positive in the cloud-interactive simulations (bold black diamond). The essential role of clouds in shaping the equatorial Pacific zonal SST gradient is consistent with the surface energy budget analysis discussed in Section 3. ΔT_{SW} is the only term that contributes to the enhanced zonal SST gradient over the equatorial Pacific (yellow circles), supporting the hypothesis that zonally contrasting cloud feedbacks enhance the SST gradient.

In addition to direct radiative effects, the cloud effect also manifests the non-radiative effects originated from the interaction between clouds and circulations. For the triangle-shaped surface cooling that maximizes in the southeastern Pacific and extends to the central equatorial Pacific, it is produced by two parts of cloud effects together. The southeastern Pacific cooling is caused by the decrease in shortwave surface radiative flux associated with the increase in stratiform clouds (Figures 2e-f), as mentioned earlier in the discussion of the zonal SST gradient; on the other hand, the central equatorial Pacific cooling could be attributed to the increase in evaporation due to cloud effects (Figures 2c-d). We interpret the increased evaporation due to the change in clouds as part of the *indirect effects by clouds*. The increase in the zonal SST gradient associated with cloud and shortwave radiative flux changes over the tropical Pacific (Figures 2e-f) drives anomalous surface easterlies (arrows in Figures 2a-b) (Lindzen & Nigam, 1987) and leads to further increase in evaporation over the central equatorial Pacific (Figures 2c-d). Namely, the change in cloud cover ultimately drives the latent heat cooling over the central equatorial Pacific. This increased evaporation as part of the cloud effect explains a large portion of the anomalous surface latent heat flux in the cloud-interactive simulations (comparing Figures 2c-d with Figures 1c-d), and contributes to more than half of the enhancement of the interhemispheric SST gradient over the tropics (ΔSST_{NS}; Figures 2g-h). In summary, direct cloud radiative effects contribute to the zonal structure of the anomalous SST, while indirect (i.e., non-radiative) cloud effects promote the meridional structure of the anomalous SST.

One may suspect that the slab-ocean setting exaggerates the cloud effects due to lack of vertical mixing and circulation feedbacks in the ocean. It is verified in Figure 3, which shows the SST response to the North Atlantic heating with a fully interactive ocean model (FOM), that the importance of clouds can still be seen within the first few decades. The North Pacific heating experiments lead to similar conclusions (Figure S1). Despite weaker magnitudes, the SST pattern response in the FOM experiments is qualitatively similar to those in the slab-ocean experiments (compare Figure 3a with Figure 1a; also see Figure 3e). The triangle-shaped cooling over the southeastern and equatorial-central Pacific is statistically significant in the FOM experiments and is persistent till year 30 (Figures 3a-b). This cooling can be attributed to the cloud effect (Figure 3d) and is absent in the cloud-locking simulations over the first decade (Figure 3c). Shown by Figure 3f, shortwave cloud radiative effect dominates the zonal gradient of equatorial Pacific SST tendencies over the first decade, while the cloud indirect effect of latent heat flux contributes primarily to the meridional gradient of tropical SST tendencies over both the first and the third decade. The oceanic heat convergent term always damps the gradients of the SST tendencies (purple triangles in Figure 3f). These results support the existence of our proposed mechanisms in a model setting with a fully interactive ocean, with a stronger confidence over the first decade after the forcing is imposed.

5 Summary and Discussion

Kang et al. (2018) and L'Hévéder et al. (2015) report that the tropical SST pattern is insensitive to the longitudinal location of extratropical thermal forcing in a slab-ocean setting. In this study, we investigate the formation mechanisms of such tropical

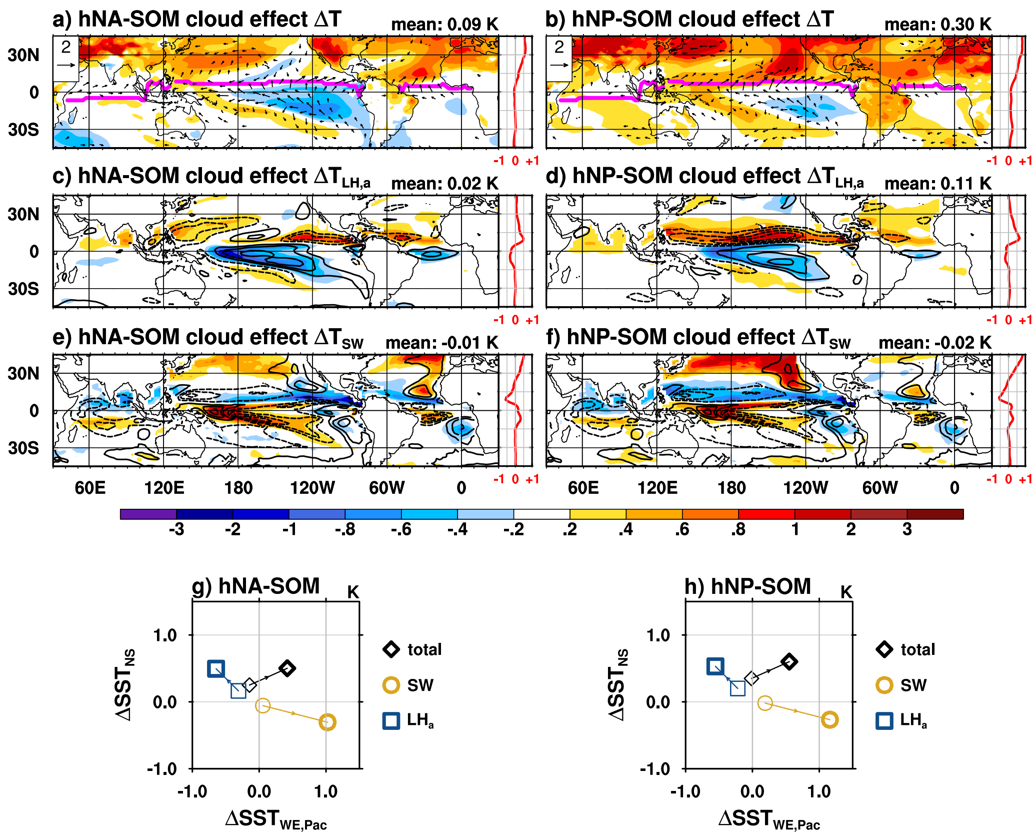

Figure 2. (a-f) as Figures 1(a-f), but of the cloud effect except for the SW-SST feedback in e-f (contours); (g-h) SST gradient metrics (see definition later in the caption) from the cloud-locking runs (thin markers) and the cloud-interactive runs (bold markers) associated with the surface fluxes labelled in the legend, where the arrows between the thin and the bold markers depict the cloud effect. The tropical meridional SST gradient (ΔSST_{NS}) is defined as the areal mean SST over 0°-20°N minus that over 20°S-0° across all longitudes; the equatorial Pacific zonal SST gradient ($\Delta SST_{WE,Pac}$) is defined as the areal mean SST over 160°E-180° minus that over 110°W-90°W within 5°S-5°N.

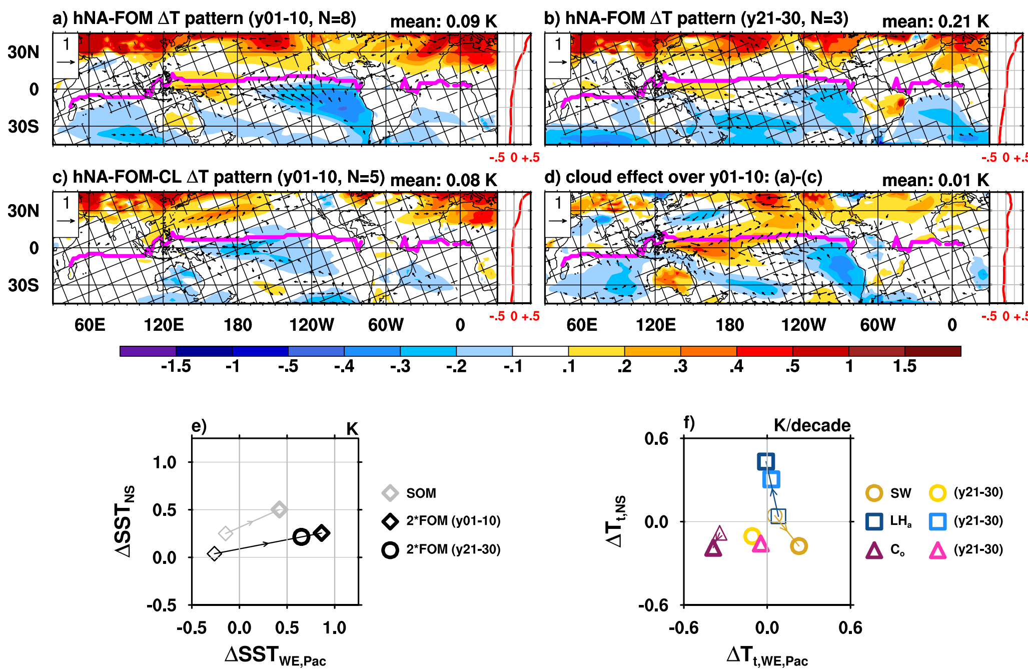

Figure 3. As Figure 1a, but of the ensemble means from the fully coupled simulations averaged over (a) years 1-10 and (b) years 21-30. (c) shows the response in the cloud-locking simulations over years 1-10 and (d) shows the corresponding cloud effect. (e) is as Figure 2e but only shows those for the overall SST gradients (fully coupled results are multiplied by two for clarity). (f) is also as Figure 2e but shows those for SST tendencies (T_t) instead of SST anomalies over years 1-10, while symbols with lighter colors represent the responses over years 21-30.

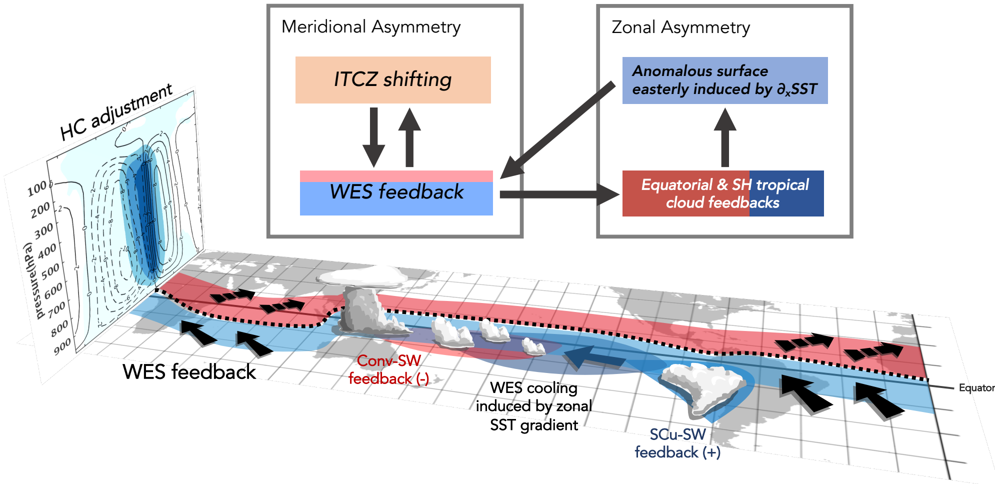

Figure 4. A schematic of the feedbacks behind the La Niña-like SST formation. Hadley Cell adjustment due to the forcing is shown on the left. On the map, the climatological ITCZ is indicated by the dashed line, with near-surface wind change (arrows) and associated SST change by the WES feedback (band-structured shading) when the ITCZ shifts north. Cloud-associated responses near the equator are also depicted with realistic style and its effects on SST response are as the shading patches. A flow chart of the discussed feedbacks is on the top.

SST pattern in CESM1. A schematic of our proposed mechanisms that lead to the common SST pattern is displayed in Figure 4. First, responding to heating in extratropical Northern Hemisphere, an anomalous cross-equatorial Hadley Cell develops. On the south of the climatological rainband, the enhanced southeasterly trades lead to enhanced evaporative cooling. With the cooling, zonally contrasting cloud cover responses emerge over the equatorial Pacific. As a result, zonal SST gradient and near-surface easterlies over the southern subtropical Pacific are strengthened. In other words, WES feedback and cloud-SST feedbacks together build up a positive feedback between the zonal and meridional structures of tropical SST changes over the tropical Pacific. This formation of the anomalous SST pattern is triggered when hemispheric differential heating is presented in the extratropics. While the energetic framework provides zonal-mean predictability under extratropical hemispheric differential heating (as summarized in Kang et al., 2020), combining our findings with the zonal homogenization of the forcing (Kang et al., 2018) yields spatial predictability of tropical responses.

The robust control of climatology fields to tropical SST response also implies that mean-state biases in CESM could lead to uncertainties regarding the mechanisms proposed in this study. However, although the mean-state biases may quantitatively influence the magnitudes of SST response, the mechanisms discussed should be at work even without a perfect climatology. For example, the WES cooling on the south of the rainband should be qualitatively similar among the GCMs with the ITCZ located on the north of the equator in most seasons. The mechanisms that link zonal to meridional SST gradient should be at work as long as the overall signs of the cloud-SST feedback pattern agree with observations over the tropics, which is true in most of the GCMs (X. Chen et al., 2019). As supportive evidence, Hwang et al. (2017) report a linear relationship between interhemispheric tropical SST asymmetry and zonal SST gradient over the southern subtropical Pacific in abrupt 4xCO_2 experiments in CMIP5 models, despite the presence of double-ITCZ biases and quantitatively inaccurate cloud-SST feedbacks in most of the models.

The importance of WES effects and cloud-SST feedbacks on extratropical-to-tropical teleconnections have been discussed extensively in the literature of seasonal footprinting mechanisms (Vimont et al., 2001), meridional modes (Chiang & Vimont, 2004), and central Pacific El Niño-Southern Oscillation (Yu et al., 2015), that anomalies of subtropical trade winds could alter latent heat flux and thus local SST gradients, leading to the propagation of SST anomalies into the deep tropics. Our result highlights the critical role of clouds in shaping such teleconnection patterns. This message is consistent with recent modeling studies suggesting that the positive cloud-SST feedback over the eastern basins could either amplify or drive SST variabilities on decadal timescales (Bellomo et al., 2014, 2015; Clement et al., 2015; Burgman et al., 2017; Middlemas et al., 2019). While literature of meridional modes mostly focuses on variabilities within individual oceanic basins, we demonstrate a cross-hemispheric influence of high-latitudinal heating on meridional mode-like response via the adjustments of Hadley Cells and the following responses of surface fluxes and clouds.

The mechanisms we reported here linking meridional to zonal SST gradient largely depend on surface fluxes in the subtropics, which is different from the mechanisms related to oceanic upwelling over the eastern equatorial Pacific proposed by previous literature (e.g. Chiang et al., 2008; Fedorov et al., 2015). It is worth noting that our FOM simulations are only run out to thirty years after the system being perturbed, and oceanic processes on longer timescales might take place and alter the response patterns if we extend the simulations (e.g. Kang et al., 2020; K. Wang et al., 2018), which is partly shown in Figure S1b. Our result at least suggests that within thirty years, when only the "fast" responses in FOM simulations are present, the mechanisms discussed are robust. The interaction between circulation, surface turbulent fluxes, and clouds should be emphasized when predicting, say, the changes in climate patterns after a few decades given certain anthropogenic climate change. The results also suggest that better representation of cloud properties over the tropics is essential for modeling the associated mechanisms and could potentially improve the predictive skill of tropical SST pattern on decadal timescales.

Open Research

CESM 1.2 can be downloaded and installed following the official documentation provided by NCAR and UCAR: `https://www.cesm.ucar.edu/models/cesm1.2/`. To reproduce the simulations, follow the details described in Text S1, including the model settings, the spatial structures of the extratropical heating, the imposed form of heating, and the procedures of how to save and impose cloud optical properties. The list of simulations is provided as Table S1.

Acknowledgments

We appreciate Dr. Paulo Ceppi for kindly providing the source codes for cloud locking in CESM1. We are also grateful to Prof. Shang-Ping Xie for his thoughtful comments. Y.-T. Hwang and Y.-J. Chen are supported by the Ministry of Science and Technology of Taiwan (MOST 110-2628-M-002-002).

References

Amaya, D. J., Kosaka, Y., Zhou, W., Zhang, Y., Xie, S.-P., & Miller, A. J. (2019, November). The north pacific pacemaker effect on historical ENSO and its mechanisms. *J. Clim.*, *32*(22), 7643–7661.

Andrews, T., Gregory, J. M., & Webb, M. J. (2015, February). The dependence of radiative forcing and feedback on evolving patterns of surface temperature

change in climate models. *J. Clim.*, *28*(4), 1630–1648.
Bellomo, K., Clement, A. C., Mauritsen, T., Rädel, G., & Stevens, B. (2014, July). Simulating the role of subtropical stratocumulus clouds in driving pacific climate variability. *J. Clim.*, *27*(13), 5119–5131.
Bellomo, K., Clement, A. C., Mauritsen, T., Rädel, G., & Stevens, B. (2015, April). The influence of cloud feedbacks on equatorial atlantic variability. *J. Clim.*, *28*(7), 2725–2744.
Burgman, R. J., Kirtman, B. P., Clement, A. C., & Vazquez, H. (2017, January). Model evidence for low-level cloud feedback driving persistent changes in atmospheric circulation and regional hydroclimate: Role of low clouds in PDV and U.S. drought. *Geophys. Res. Lett.*, *44*(1), 428–437.
Ceppi, P., & Gregory, J. M. (2017, December). Relationship of tropospheric stability to climate sensitivity and earth's observed radiation budget. *Proc. Natl. Acad. Sci. U. S. A.*, *114*(50), 13126–13131.
Ceppi, P., & Hartmann, D. L. (2016, January). Clouds and the atmospheric circulation response to warming. *J. Clim.*, *29*(2), 783–799.
Chen, X., Guo, Z., Zhou, T., Li, J., Rong, X., Xin, Y., ... Su, J. (2019, February). Climate sensitivity and feedbacks of a new coupled model CAMS-CSM to idealized CO2 forcing: A comparison with CMIP5 models. *J. Meteorol. Res.*, *33*(1), 31–45.
Chen, Y.-J., Hwang, Y.-T., & Ceppi, P. (2021, October). The impacts of Cloud-Radiative changes on poleward atmospheric and oceanic energy transport in a warmer climate. *J. Clim.*, *34*(19), 7857–7874.
Chiang, J. C. H., & Bitz, C. M. (2005, October). Influence of high latitude ice cover on the marine intertropical convergence zone. *Clim. Dyn.*, *25*(5), 477–496.
Chiang, J. C. H., Fang, Y., & Chang, P. (2008, July). Interhemispheric thermal gradient and tropical pacific climate. *Geophys. Res. Lett.*, *35*(14).
Chiang, J. C. H., & Vimont, D. J. (2004, November). Analogous pacific and atlantic meridional modes of tropical Atmosphere–Ocean variability. *J. Clim.*, *17*(21), 4143–4158.
Clement, A. C., Bellomo, K., Murphy, L. N., Cane, M. A., Mauritsen, T., Rädel, G., & Stevens, B. (2015, October). The atlantic multidecadal oscillation without a role for ocean circulation. *Science*, *350*(6258), 320–324.
Clement, A. C., Seager, R., Cane, M. A., & Zebiak, S. E. (1996, September). An ocean dynamical thermostat. *J. Clim.*, *9*(9), 2190–2196.
Collins, M., Minobe, S., Barreiro, M., Bordoni, S., Kaspi, Y., Kuwano-Yoshida, A., ... Zolina, O. (2018, January). Challenges and opportunities for improved understanding of regional climate dynamics. *Nat. Clim. Chang.*, *8*(2), 101–108.
Delworth, T. L., Zeng, F., Rosati, A., Vecchi, G. A., & Wittenberg, A. T. (2015, May). A link between the hiatus in global warming and north american drought. *J. Clim.*, *28*(9), 3834–3845.
DiNezio, P. N., Clement, A. C., Vecchi, G. A., Soden, B. J., Kirtman, B. P., & Lee, S.-K. (2009, September). Climate response of the equatorial pacific to global warming. *J. Clim.*, *22*(18), 4873–4892.
Dong, Y., Proistosescu, C., Armour, K. C., & Battisti, D. S. (2019, September). Attributing historical and future evolution of radiative feedbacks to regional warming patterns using a green's function approach: The preeminence of the western pacific. *J. Clim.*, *32*(17), 5471–5491.
Fedorov, A. V., Burls, N. J., Lawrence, K. T., & Peterson, L. C. (2015, December). Tightly linked zonal and meridional sea surface temperature gradients over the past five million years. *Nat. Geosci.*, *8*(12), 975–980.
Hanson, H. P. (1991, March). Marine stratocumulus climatologies. *Int. J. Climatol.*, *11*(2), 147–164.
Heede, U. K., Fedorov, A. V., & Burls, N. J. (2020, July). Time scales and mechanisms for the tropical pacific response to global warming: A tug of war be-

tween the ocean thermostat and weaker walker. *J. Clim.*, *33*(14), 6101–6118.
Hurrell, J. W., Holland, M. M., Gent, P. R., Ghan, S., Kay, J. E., Kushner, P. J., ... Marshall, S. (2013, September). The community earth system model: A framework for collaborative research. *Bull. Am. Meteorol. Soc.*, *94*(9), 1339–1360.
Hwang, Y.-T., Tseng, H.-Y., Li, K.-C., Kang, S. M., Chen, Y.-J., & Chiang, J. C. H. (2021, May). Relative roles of energy and momentum fluxes in the tropical response to extratropical thermal forcing. *J. Clim.*, *34*(10), 3771–3786.
Hwang, Y.-T., Xie, S.-P., Deser, C., & Kang, S. M. (2017, September). Connecting tropical climate change with southern ocean heat uptake. *Geophys. Res. Lett.*, *44*(18), 9449–9457.
Kang, S. M., Held, I. M., & Xie, S.-P. (2014). Contrasting the tropical responses to zonally asymmetric extratropical and tropical thermal forcing. *Clim. Dyn.*.
Kang, S. M., Park, K., Hwang, Y.-T., & Hsiao, W.-T. (2018, November). Contrasting tropical climate response pattern to localized thermal forcing over different ocean basins. *Geophys. Res. Lett.*, *45*(22), 12,544–12,552.
Kang, S. M., Xie, S.-P., Shin, Y., Kim, H., Hwang, Y.-T., Stuecker, M. F., ... Hawcroft, M. (2020, November). Walker circulation response to extratropical radiative forcing. *Sci Adv*, *6*(47).
Klein, S. A., & Hartmann, D. L. (1993, August). The seasonal cycle of low stratiform clouds. *J. Clim.*, *6*(8), 1587–1606.
Lau, K.-M., Wu, H.-T., & Bony, S. (1997, March). The role of Large-Scale atmospheric circulation in the relationship between tropical convection and sea surface temperature. *J. Clim.*, *10*(3), 381–392.
L'Hévéder, B., Codron, F., & Ghil, M. (2015, April). Impact of anomalous northward oceanic heat transport on global climate in a slab ocean setting. *J. Clim.*, *28*(7), 2650–2664.
Lindzen, R. S., & Nigam, S. (1987, September). On the role of sea surface temperature gradients in forcing Low-Level winds and convergence in the tropics. *J. Atmos. Sci.*, *44*(17), 2418–2436.
Luo, Y., Lu, J., Liu, F., & Garuba, O. (2017, April). The role of ocean dynamical thermostat in delaying the el niño–like response over the equatorial pacific to climate warming. *J. Clim.*, *30*(8), 2811–2827.
Meehl, G. A., & Washington, W. M. (1996, July). El niño-like climate change in a model with increased atmospheric CO2 concentrations. *Nature*, *382*(6586), 56–60.
Middlemas, E. A., Clement, A. C., Medeiros, B., & Kirtman, B. (2019, August). Cloud radiative feedbacks and el niño–southern oscillation. *J. Clim.*, *32*(15), 4661–4680.
Neale, R. B., Chen, C.-C., Gettelman, A., Lauritzen, P. H., Park, S., Williamson, D. L., ... Others (2010). Description of the NCAR community atmosphere model (CAM 5.0). *NCAR Tech. Note NCAR/TN-486+ STR*, *1*(1), 1–12.
Park, C., Kang, S. M., Stuecker, M. F., & Jin, F.-F. (2022, January). Distinct surface warming response over the western and eastern equatorial pacific to radiative forcing. *Geophys. Res. Lett.*.
Ramanathan, V., & Collins, W. (1991, May). Thermodynamic regulation of ocean warming by cirrus clouds deduced from observations of the 1987 el niño. *Nature*, *351*(6321), 27–32.
Shin, Y., Kang, S. M., Takahashi, K., Stuecker, M. F., Hwang, Y.-T., & Kim, D. (2021, August). Evolution of the tropical response to periodic extratropical thermal forcing. *J. Clim.*, *34*(15), 6335–6353.
Stevens, B., Sherwood, S. C., Bony, S., & Webb, M. J. (2016, November). Prospects for narrowing bounds on earth's equilibrium climate sensitivity. *Earths Future*, *4*(11), 512–522.
Vimont, D. J., Battisti, D. S., & Hirst, A. C. (2001, October). Footprinting: A sea-

sonal connection between the tropics and mid-latitudes. *Geophys. Res. Lett.*, *28*(20), 3923–3926.
Wang, K., Deser, C., Sun, L., & Tomas, R. A. (2018, May). Fast response of the tropics to an abrupt loss of arctic sea ice via ocean dynamics. *Geophys. Res. Lett.*, *45*(9), 4264–4272.
Wang, L., & Huang, K. (2016, April). Imprint of the ENSO on rainfall and latent heating variability over the southern south china sea from TRMM observations. *J. Ocean Univ. China*, *15*(2), 219–231.
Wei, W., Li, W., Deng, Y., Yang, S., Jiang, J. H., Huang, L., & Liu, W. T. (2018, April). Dynamical and thermodynamical coupling between the north atlantic subtropical high and the marine boundary layer clouds in boreal summer. *Clim. Dyn.*, *50*(7), 2457–2469.
Xie, S.-P. (2020, March). Ocean warming pattern effect on global and regional climate change. *AGU Advances*, *1*(1).
Xie, S.-P., Deser, C., Vecchi, G. A., Ma, J., Teng, H., & Wittenberg, A. T. (2010, February). Global warming pattern formation: Sea surface temperature and rainfall. *J. Clim.*, *23*(4), 966–986.
Yu, J.-Y., Kao, P.-K., Paek, H., Hsu, H.-H., Hung, C.-W., Lu, M.-M., & An, S.-I. (2015, January). Linking emergence of the central pacific el niño to the atlantic multidecadal oscillation. *J. Clim.*, *28*(2), 651–662.
Zhang, H., Clement, A., & Di Nezio, P. (2014, January). The south pacific meridional mode: A mechanism for ENSO-like variability. *J. Clim.*, *27*(2), 769–783.
Zhang, L., & Li, T. (2014, November). A simple analytical model for understanding the formation of sea surface temperature patterns under global warming. *J. Clim.*, *27*(22), 8413–8421.
Zhao, J., Zhan, R., & Wang, Y. (2018, April). Global warming hiatus contributed to the increased occurrence of intense tropical cyclones in the coastal regions along east asia. *Sci. Rep.*, *8*(1), 6023.

Supporting Information for "The Role of Clouds in Shaping Tropical Pacific Response Pattern to Extratropical Thermal Forcing"

Wei-Ting Hsiao[1,2], Yen-Ting Hwang[1], Yong-Jhih Chen[1], and Sarah M. Kang[3]

[1]Department of Atmospheric Sciences, National Taiwan University, Taipei, Taiwan

[2]Department of Atmospheric Science, Colorado State University, Fort Collins, CO, USA

[3]School of Urban and Environmental Engineering, Ulsan National Institute of Science and Technology, Ulsan, South Korea

Contents of this file

1. Text S1 to S2
2. Figure S1
3. Table S1

Introduction The supporting information includes (1) a section of text describing experimental settings in detail, (2) a supplementary figure that is mentioned but not present in the main text, and (3) a table that describe all the simulations that were conducted.

Text S1. Model setting

S1.1 Experimental Design

Community Earth System Model 1.2 (CESM 1.2; Hurrell et al., 2013) has been employed to perform the experiments in this study. The atmospheric model, Community Atmosphere Model 5.0 (CAM5; Neale et al., 2010), is used with an active seasonal cycle and spatial resolution of 1.9° latitude by 2.5° longitude and 30 vertical layers. Realistic continental distribution and topography is used. Vegetation, aerosols, and greenhouse gases are set to pre-industrial conditions. The oceanic model, Parallel Ocean Program 2.0 (POP2), is used with the grid system of gx1v6, which is approximately 1° by 1° horizontally.

In the slab-ocean setting, the default POP2 grid in vertical direction is replaced by a single-layer slab ocean of a homogeneous depth of 50 meters. A q flux with seasonal cycle obtained by the time-mean data of the control run in a fully coupled setting, which represents the convergence of climatological oceanic heat transport, are prescribed in the slab ocean. Dynamical oceanic interactions with other components of the model are absent in this setting. A control simulation (CTL) using the historical scenario of the 1850s is performed. Two perturbed simulations are branched from a same arbitrary year of CTL, in which the surface heating is imposed into the slab ocean as additional q flux over either the Northern Atlantic (hNA) and the Northern Pacific (hNP). The heating is roughly imposed between 45°N and 65°N zonally uniformly with a meridional half-sine shape. The peak values of the heating are about 69.5 W m^{-2}, and the total amount of each heating field is adjusted to be approximately 0.41 petawatts by modifying the latitudinal range slightly. Note that the area of heating avoids where the annual maximum sea ice cover is over 0.5 to prevent severe effects from direct melting of ice. For the time length that each simulation has been run out to, see Table S1. The perturbed simulations have reached equilibria with the time ran as their global mean imbalances of top-of-the-atmosphere (TOA) flux lie within positive and negative 0.15 W m^{-2}, which is similar to the value from CTL (0.13 W m^{-2}). To reproduce the simulations, use the *compset* E1850C5.

To investigate cloud radiative effects, we use a cloud-locking (CL) method in CAM5 (Ceppi & Hartmann, 2016; Chen et al., 2021) with the slab-ocean setting to verify the role of clouds. Hourly cloud optical properties of the control run are prescribed in the simulations of cloud locking. A control simulation (CTL-CL) is performed, which is branched from an arbitrary year in CTL and cloud radiative properties from CTL are then being imposed from another arbitrary year in CTL to capture the decoupling effect between cloud radiative properties and other fields. Two perturbed simulations (hNA-CL and hNP-CL) are branched from a same arbitrary year in CTL, when the idealized surface heating and the CTL cloud optical properties are started to be imposed. Similarly, the perturbed simulations have reached equilibria that their global mean imbalances of TOA flux lie within 0.11 W m^{-2}, which are similar to the value from CTL-CL (0.11 W m^{-2}). We could then obtain the responses to heating without cloud effect by subtracting any fields from CTL-CL from either hNA-CL or hNP-CL. Finally, the cloud effect is obtained by subtracting the responses to heating with cloud effect by those without cloud effect.

We also conduct a set of fully coupled (FOM) experiments with two idealized forcing to investigate the importance of the processes discussed in the slab-ocean experiments with oceanic dynamical responses. The ocean model is set to be dynamically interactive with 60 vertical layers and with realistic oceanic topography. A control simulation (CTL-FOM) is performed. In the perturbed simulations (hNA-FOM and hNP-FOM), the idealized surface heating is imposed in the form of additional downward longwave radiative flux with the horizontal spatial structures same as in the slab-ocean heating simulations. To show the transient responses to the extratropical forcing, multiple ensembles of FOM heating experiments are performed (see Table S1 for detail). To reproduce the simulations, use the *compset* B1850C5.

S1.2 Technical details of implementing cloud locking

In the radiation scheme of CAM5 (RRTMG; Iacono et al., 2008), a number of cloud properties are used in the calculation of radiative fluxes (Pincus et al., 2003). Those variables include cloud fraction, snow cloud fraction, in-cloud liquid/ice/snow water path, effective diameter for ice and snow, and size distribution parameters. From the control simulations (CTL-SOM and CTL-FOM), we save the instantaneous fields of these variables whenever the radiation module is called (i.e., every hour). Next, in the cloud-locking simulations, we prescribe the cloud properties in the radiation calculation with the cloud fields saved beforehand. This is done by overwriting the cloud properties in the following subroutines:

1. radiation_tend
2. get_liquid_optics_sw
3. get_ice_optics_sw
4. get_snow_optics_sw

5. snow_cloud_get_rad_props_lw
6. ice_cloud_get_rad_props_lw
7. liquid_cloud_get_rad_props_lw

By doing so, the radiation module would always use the prescribed cloud properties in the calculation of radiative fluxes, instead of the cloud properties in the current simulation.

Text S2. The derivation of the attribution of SST anomalies to surface and oceanic mixed-layer energy fluxes

An energy budget analysis of oceanic mixed layer is used to attribute SST response to each surface energy flux (Xie et al., 2010; Zhang & Li, 2014). First, we assume that the temperature is uniform across the mixed layer including its surface. The time tendency of the mixed-layer temperature (T) can be written as:

$$T_t = \frac{1}{\rho c_p H} \left(Q_{SW} + Q_{LW} + Q_{LH} + Q_{SH} + Q_{C_o} \right)$$

where subscript t denotes time derivative, the density of sea water, c_p the specific heat capacity at constant pressure of sea water, H the mixed-layer depth, and Q the inward energy flux. Fluxes include shortwave (SW) and longwave (LW) radiative fluxes, latent heat flux (LH), sensible heat flux (SH), and column-integrated heat convergence by the transport of ocean currents (C_o), with the sign convention that positive heats the surface. Since Q_{C_o} is not directly provided by the model, it is calculated by the following formula:

$$Q_{C_o} = -\int_{-H}^{surface} \nabla \cdot \left(\vec{V} H_{OHC} \right) dz$$

where H denotes mixed-layer depth, $\vec{V}$ is oceanic current, and H_{OHC} is the oceanic heat content. Here, the mean H of the forced states and the control state are used, so the effect of the change in mixed layer thickness is omitted during the calculation. Another step to note is that the model output H is continuous while the ocean vertical grid points are discrete and scarce compared to the change in H, thus the vertical integral is calculated assuming that the vertical variations of $\vec{V}$ and H_{OHC} are linear between the grid points.

In SOM experiments, Q_{C_o} is unchanged by design (represented as q flux) and the system reaches equilibrium thus the total $T_t = 0$. The temperature difference between the control state and the forced state could be written as:

$$\Delta T_{flux} = \frac{1}{\overline{dQ/dT}} \Delta Q_{flux}, \quad flux = \{SW, LW_{dn}, LH_a, SH\}$$

where Δ denotes the differences between the forced state and the control state, $\overline{dQ/dT}$ is the linear dependence of total surface energy flux to T evaluated at the mean states between the forced and the control states, which consists of a blackbody longwave radiative term ($4\sigma T^3$) and a latent heat term associated with its bulk formula ($L_v Q_{LH}/RT^2$). Note that sensible heat flux also has a linear dependency on the surface temperature, but is omitted because its high nonlinearity leads to unreasonable magnitudes of values when implementing our calculation procedure. After removing the linear dependent terms to T, downward longwave radiative flux (LW_{dn}) and non-Newtonian latent heat flux that depends solely on near-surface atmospheric condition (LH_a) appear that replace LW and LH, respectively. The complete expression of ΔT_{flux} is:

$$\Delta T_{flux} = \frac{1}{4\sigma \bar{T}^3 + L_v \overline{Q_{LH}}/R\bar{T}^2} \Delta Q_{flux}, \quad flux = \{SW, LW_{dn}, LH_a, SH\}$$

where the overbar denotes the mean states of the forced and the control states (simply calculated as the arithmetic means of the two states) as this method is essentially utilizing a Taylor's expansion with respect to a certain state. Finally, we note that all the calculations are done for each calendar month and annual means are calculated as the final step.

References

Ceppi, P., & Hartmann, D. L. (2016, January). Clouds and the atmospheric circulation response to warming. *J. Clim.*, *29*(2), 783–799.

Chen, Y.-J., Hwang, Y.-T., & Ceppi, P. (2021, October). The impacts of Cloud-Radiative changes on poleward atmospheric and oceanic energy transport in a warmer climate. *J. Clim.*, *34*(19), 7857–7874.

Hurrell, J. W., Holland, M. M., Gent, P. R., Ghan, S., Kay, J. E., Kushner, P. J., ... Marshall, S. (2013, September). The community earth system model: A framework for collaborative research. *Bull. Am. Meteorol. Soc.*, *94*(9), 1339–1360.

Iacono, M. J., Delamere, J. S., Mlawer, E. J., Shephard, M. W., Clough, S. A., & Collins, W. D. (2008, July). Radiative forcing by long-lived greenhouse gases: Calculations with the AER radiative transfer models. *J. Geophys. Res.*, *113*(D13).

Neale, R. B., Chen, C.-C., Gettelman, A., Lauritzen, P. H., Park, S., Williamson, D. L., ... Others (2010). Description of the NCAR community atmosphere model (CAM 5.0). *NCAR Tech. Note NCAR/TN-486+ STR*, *1*(1), 1–12.

Pincus, R., Barker, H. W., & Morcrette, J.-J. (2003, July). A fast, flexible, approximate technique for computing radiative transfer in inhomogeneous cloud fields. *J. Geophys.*

Res., *108*(D13).

Xie, S.-P., Deser, C., Vecchi, G. A., Ma, J., Teng, H., & Wittenberg, A. T. (2010, February). Global warming pattern formation: Sea surface temperature and rainfall. *J. Clim.*, *23*(4), 966–986.

Zhang, L., & Li, T. (2014, November). A simple analytical model for understanding the formation of sea surface temperature patterns under global warming. *J. Clim.*, *27*(22), 8413–8421.

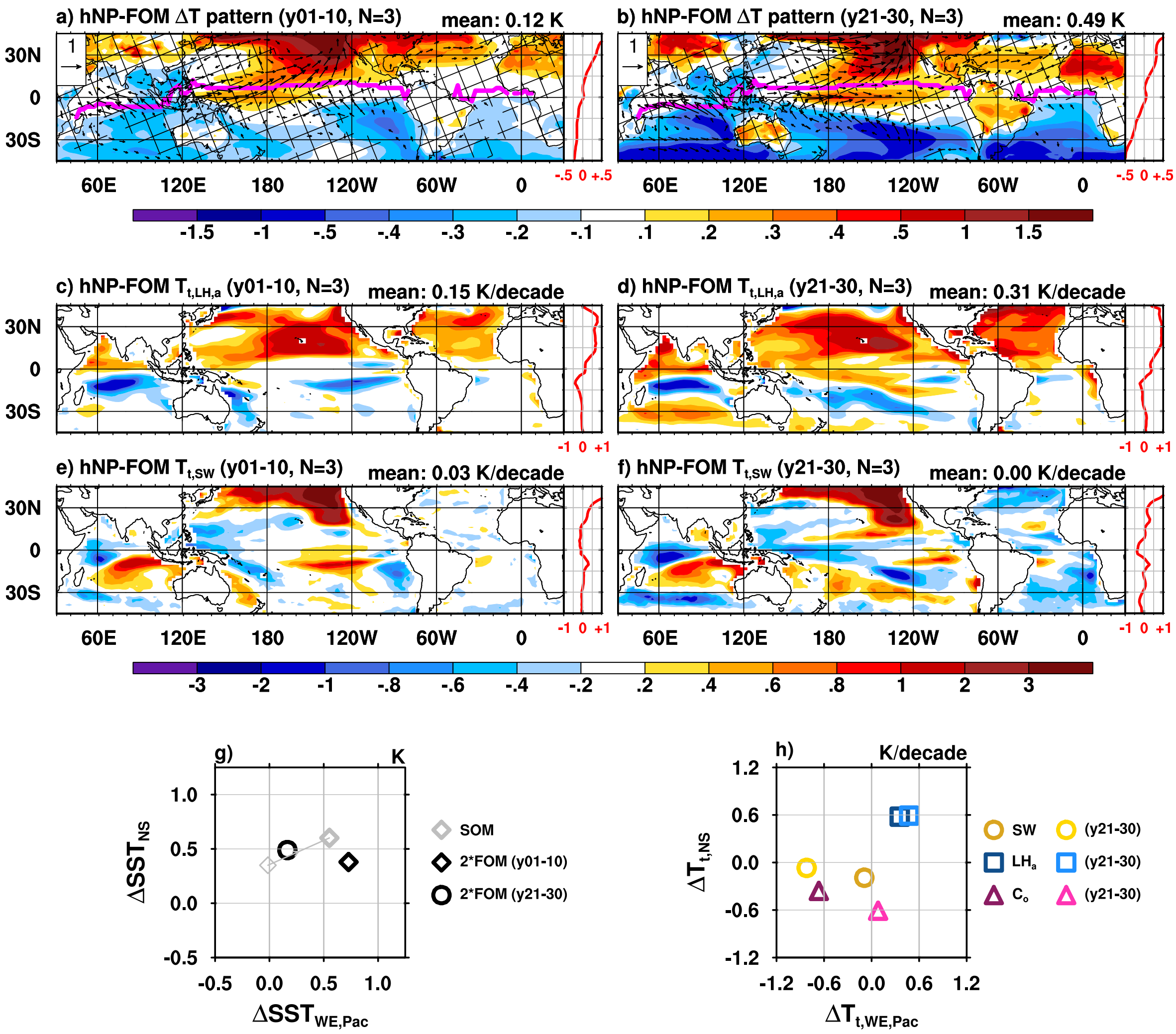

Figure S1. Results from the fully coupled North Pacific heating experiments (hNP-FOM): (a-b) as Figures 4a-b; color shadings in (c-d) are as Figures 2d and (e-f) are as Figures 2f, but of the associated SST tendencies (K decade^{-1}) over the two time periods; (g-h) as Figures 4e-f. Note that the SST gradient metrics are not perfectly suitable for presenting the results from hNP-FOM runs: for example, in (h) the SST tendency contributed by SW does not enhance the $\Delta T_{t,WE,Pac}$ over the first ten years, however, a clear spatial pattern of $T_{t,SW}$ that follows the climatological cloud regime is shown in (e) that enhances the zonal SST gradient locally over the central and the eastern tropical Pacific. We argue that the mechanisms of the SST pattern formation that highlight the importance of clouds proposed in the main text are still important here, but are manifested differently with a more complicated spatial distribution of SST-cloud feedbacks.

Table S1. The experiment list

Name	Descriptions	Simulated Years	Years Analyzed	Ensemble Counts
CTL-SOM	Preindustrial control simulation with a slab-ocean lower boundary	95	70	1
hNA-SOM	Surface thermal heating added in the extratropical North Atlantic with a slab-ocean lower boundary	65	30	1
hNP-SOM	As hNA-SOM but with extratropical North Pacific heating	65	30	1
CTL-SOM-CL	As CTL-SOM but cloud properties are locked to those in different years from CTL-SOM	40	30	1
hNA-SOM-CL	As hNA-SOM but cloud properties are locked to those from CTL-SOM	40	20	1
hNP-SOM-CL	As hNP-SOM but cloud properties are locked to those from CTL-SOM	40	20	1
CTL-FOM	Preindustrial control simulation with a dynamical-ocean lower boundary	120	120	1
hNA-FOM	Surface thermal heating added in the extratropical North Atlantic with a dynamical-ocean lower boundary	30	1-10 21-30	8 (year 1-10) 3 (year 21-30)
hNP-FOM	As hNA-FOM but with extratropical North Pacific heating	30	1-10 21-30	3 (year 1-10) 3 (year 21-30)
CTL-FOM-CL	As CTL-FOM but cloud properties are locked to those in different years from CTL-FOM	10	1-10	5
hNA-FOM-CL	As hNA-FOM but cloud properties are locked to those in different years from CTL-FOM	10	1-10	5